Available online at www.sciencedirect.com
ScienceDirect
Journal of Power Sources 175 (2008) 664–668
JOURNAL OF POWER SOURCES
www.elsevier.com/locate/jpowsour

Short communication

Modelling of the thermal behaviour of an ultracapacitor for a 42-V automotive electrical system

Dae Hun Lee [a], Ui Seong Kim [a], Chee Burm Shin [a,*], Baek Haeng Lee [b], Byung Woo Kim [b], Young-Ho Kim [c]

[a] *Department of Chemical Engineering and Division of Energy Systems Research, Ajou University, Suwon 443-749, Republic of Korea*
[b] *Electronics System Development Laboratory, Korea Automotive Technology Institute, Cheonan 330-912, Republic of Korea*
[c] *NESSCAP Co., Ltd., Yongin 449-901, Republic of Korea*

Received 5 July 2007; received in revised form 6 September 2007; accepted 17 September 2007
Available online 2 October 2007

Abstract

A three-dimensional modelling approach is used to study the effects of operating and ambient conditions on the thermal behaviour of a NESSCAP 2.7 V/3500 F ultracapacitor cell for a 42-V automotive electrical system. The rate of heat generation of the ultracapacitor during charge and discharge is measured with a calorimeter. The transient temperature distribution of the ultracapacitor during cycling is obtained by using the finite element method with an implicit predictor-multicorrector algorithm. The results show that the temperature of the ultracapacitor cell increases during the first 50 cycles after which it reaches a periodic steady-state value that increases with increasing ambient temperature.

Keywords: Ultracapacitor; Thermal behaviour; Model; 42-V automotive electrical system; Finite element method

1. Introduction

Ultracapacitors, also known as supercapacitors, have the potential to meet the increasing power requirements of energy-storage systems for automotive applications [1]. Compared with batteries, ultracapacitors offer higher specific power, higher efficiency, and longer shelf- and cycle-life. The primary disadvantage of ultracapacitors is their low specific energy relative to that of batteries [2]. Although ultracapacitors have generally been considered to be in competition with batteries for use in automotive applications, a number of automotive power networks have been proposed in which both are used [1,3–6]. In such a combined strategy, batteries support the bulk energy requirements of the vehicle, whilst ultracapacitors are used to provide the majority of the peak-current output and sink requirements.

42-V automotive electrical systems provide stop–start, launch-assist, and power-assist as well as new comfort and driveability ancillaries according to the configuration of the electrical system [7,8]. A 42-V automotive power source comprising a module consisting of 2.7 V/3500 F ultracapacitors and a 36 V/20 Ah valve-regulated lead–acid (VRLA) battery is being developed by a research consortium led by the Korea Automotive Technology Institute. In order to ensure the durability and safety of such a system, thermal modelling of the ultracapacitor cell can play a vital role in maintaining the operating temperature and the temperature uniformity of the ultracapacitor module within a suitable range. In this work, the rate of heat generation of the ultracapacitor cell during charge and discharge is measured with a calorimeter. Then, based on this measurement data, a three-dimensional modelling is carried-out to investigate the effects of the operating and ambient conditions on the thermal behaviour of a NESSCAP 2.7 V/3500 F ultracapacitor cell for a 42-V automotive electrical system.

2. Mathematical model

The external appearance of the NESSCAP 2.7 V/3500 F ultracapacitor cell is shown in Fig. 1. It is divided into three major

* Corresponding author. Tel.: +82 31 219 2388; fax: +82 31 219 1612.
E-mail address: cbshin@ajou.ac.kr (C.B. Shin).

0378-7753/$ – see front matter © 2007 Elsevier B.V. All rights reserved.
doi:10.1016/j.jpowsour.2007.09.081

Fig. 1. NESSCAP 2.7 V/3500 F ultracapacitor cell.

regions: the case, the core and the gas regions. The case is constructed from aluminum and its exterior surface is coated with plastic. The core region is comprised of the stack of electrodes and separators immersed in the electrolyte. There is a small volume of gas above the core region and underneath the top cover, where the positive and negative terminals and a vent are installed. The following assumptions are made to simplify the mathematical analysis of the problem.

(i) Because the liquid electrolytes are trapped in the porous electrodes and separators of the core region, the convective heat transfer in the core region can be neglected [9]. Moreover, the gas in the gas region is assumed to be stagnant, because the gas region is sufficiently small for natural convection to take place freely. Therefore, conduction is the main mechanism of heat transfer in the cell.

(ii) In the cell, heat is generated due to ohmic losses in the whole electric circuit and the charge and discharge processes at the interfaces of the electrodes. This heat generation is non-uniformly distributed, due to the heterogeneous structure of the cell from a microscopic viewpoint. From a macroscopic viewpoint, however, the thicknesses of each electrode and separator are very small compared with the whole dimensions of the core region, so that heat generation is uniform throughout the core region during the charge and the discharge processes [10].

(iii) The effective thermal conductivities of the various compartments of the cell can be estimated based on equivalent networks of parallel and series thermal resistances of the cell components [9–11].

With the above assumptions, the transient three-dimensional equation of heat conduction can be written as follows:

$$\rho C_p \frac{\partial T}{\partial t} = \frac{\partial}{\partial x}\left(k_x \frac{\partial T}{\partial x}\right) + \frac{\partial}{\partial x}\left(k_y \frac{\partial T}{\partial y}\right) + \frac{\partial}{\partial x}\left(k_z \frac{\partial T}{\partial z}\right) + Q \quad (1)$$

where ρ is the density; C_p is the heat capacity at constant pressure; T is the temperature; t is the time; k_x, k_y, and k_z are the effective thermal conductivities along the x, y, and z directions, respectively; Q is the heat generation rate per unit volume. The physical properties used for the calculations are listed in Table 1.

3. Measurement of heat generation

Since most commercial calorimeters are manufactured for testing small cells (smaller than size C), a large, custom-made calorimeter was used to measure the heat generated by the ultracapacitor during charge and discharge. The external appearance of the calorimeter is shown in Fig. 2(a), whereas the internal configuration of the calorimeter is shown in Fig. 2(b). The calorimeter consists of two chambers. The outer chamber plays the role of a heat sink and is placed in a constant temperature and humidity vessel to keep the temperature of the heat sink constant. The vessel is controlled by a microprocessor with an accuracy of ±0.3 °C and ±1.5% relative humidity, respectively. The inner chamber, which can be seen in Fig. 2(b), contains the sample. The outer and inner chambers are made of aluminum and their approximate dimensions are 13 cm × 8 cm × 20 cm and 28 cm × 21 cm × 32 cm, respectively. Large-gauge leads, which generate a negligible amount of heat even at very high electrical

Table 1
Physical properties used for the calculations

Component	Density (g cm^{-2})	Heat capacity (J g^{-1} K^{-1})	Thermal conductivity (W cm^{-1} K^{-1})	Reference
Case	2.7	0.89815	2.37	[12]
Activated carbon	0.7	0.7	0.05	[13]
Current collector	2.7	0.89815	2.37	[12]
Electrolyte	0.7793	2.23	0.0019	[12]
Separator	0.93	1.34	0.0011	[12]
Plastic coating	1.352	0.2635	0.0016	[14]
Gas	1.1774×10^{-3}	1.0057	0.02624×10^{-2}	[12]

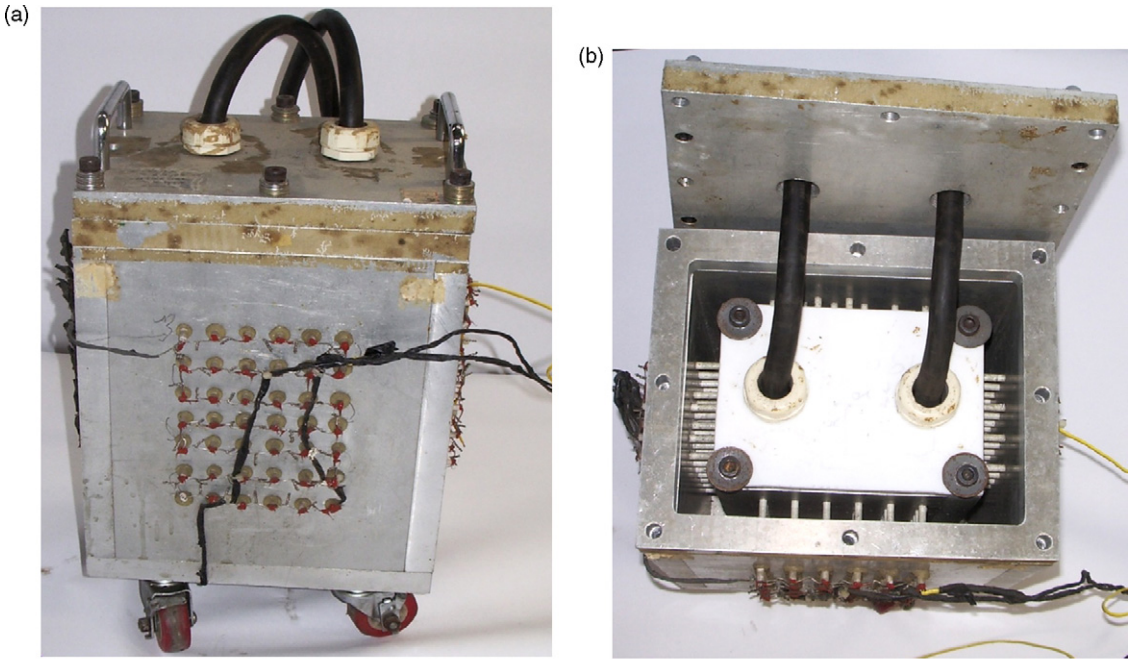

Fig. 2. Calorimeter used for measurement of heat generation: (a) external appearance and (b) internal configuration of the calorimeter.

currents, are connected to the sample through the top covers of the inner and outer chambers. If the temperature of the sample is different from that of the heat sink, heat flows between the former and the latter. Heat sensors (semiconductor thermoelectric devices) are located between the sample enclosure and the heat sink. For the calibration, an electrical heater of known resistance is used to produce heat input rates that range from 1 to 100 W.

A battery cycle-life test system from Bitrode (LCN 6-100-12) is used to charge and discharge the ultracapacitor. The system provides voltages and currents of up to 18 V and 100 A, respectively, with an accuracy of ±0.1% of full scale. The charge and discharge processes of the ultracapacitor consist of four steps. The first step is a constant-current discharge mode that ends at a given cut-off voltage. The second step consists of rest mode for 7 h. The third step is a constant-current charge mode that ends at a given floating voltage. The fourth step is a constant-voltage charge mode for 2 h. Normally, the current in the fourth step is less than 1 A, in order to prevent overcharging. The purpose of the fourth step is to enable the ultracapacitor to reach a high state of charge or to refresh it. The constant-current discharge and charge in the first and third steps, respectively, are carried out with various currents, viz. 20, 50, and 100 A. The heat generation data measured at 25 °C are given in Table 2.

4. Results and discussion

The transient temperature distribution of the ultracapacitor was obtained using the finite element method. The computational domain was discretized into 6788 tri-linear hexahedral elements that had a total of 7984 nodes. The finite element mesh used for the calculation is shown in Fig. 3. The element mesh is made denser around the region where steeper temperature gradients are to be expected. The time integration was performed using an implicit predictor-multicorrector algorithm [15].

For modelling the thermal behaviour of the ultracapacitor, a test cycle was applied to an ultracapacitor module composed of

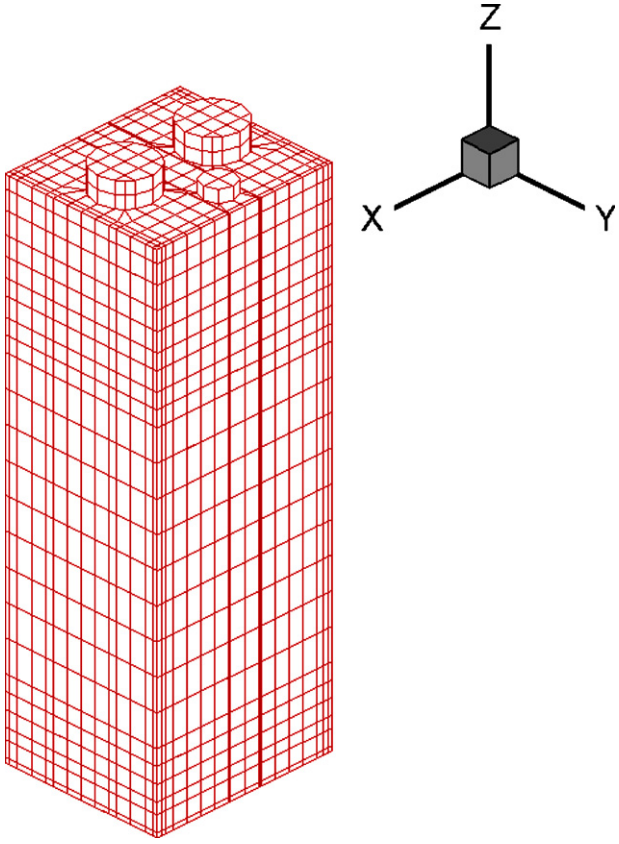

Fig. 3. Finite element mesh of ultracapacitor cell.

Table 2
Heat generation data measured by calorimetry

Operation mode	Current (A)	Time (s)	Power (W)	Heat generation (W)
Discharge	20	569	22.6979	0.0718
	50	208	53.7447	0.1319
	100	103	98.2752	0.1681
Charge	20	690	27.4661	0.1611
	50	336	60.9078	0.1899
	100	215	116.0779	0.2301

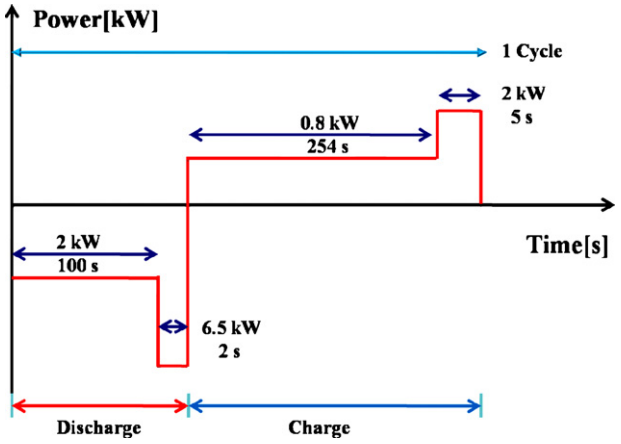

Fig. 4. Test cycle for 42-V automotive electrical system.

18 2.7 V/3500 F ultracapacitors electrically connected in series. As illustrated in Fig. 4, the test cycle consists of the following four steps: (i) an idle-stop mode with a discharge power of 2 kW for 100 s designed to operate all electrical ancillaries including air-conditioning; (ii) an acceleration mode with a discharge power of 6.5 kW for 2 s; (iii) a driving mode with a charge power of 0.8 kW for 254 s; (iv) a regenerative-braking mode with a charge power of 2 kW for 5 s. In a 42-V automotive power source that consists of an ultracapacitor module and a VRLA battery, the electrical loads will be distributed between the ultracapacitor module and the battery during power cycling according to the balancing algorithm of the electrical energy-management system of the vehicle. In this study, the entire electrical load was assumed to be carried by the ultracapacitor module, in order to model the thermal behaviour of the ultracapacitor under the most severe conditions.

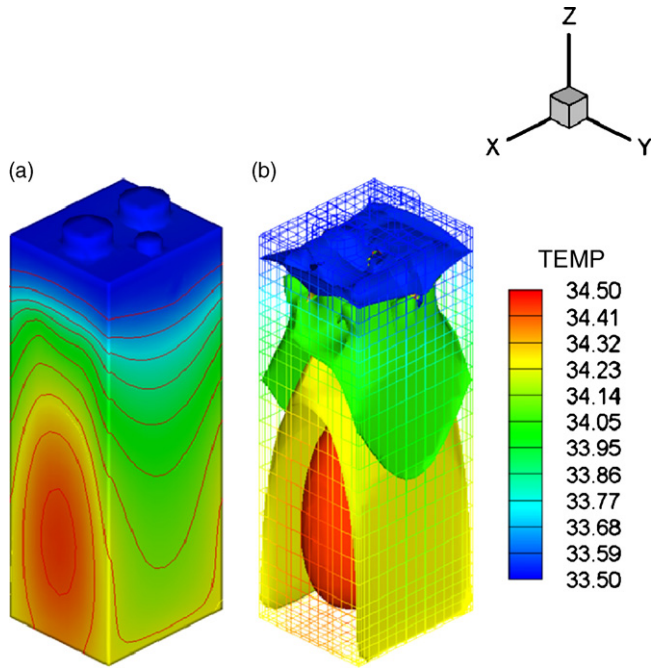

Fig. 6. (a) Surface temperature distribution and (b) isothermal surfaces distribution of cell after 50 cycles.

Fig. 5(a and b) shows the temperature transition of the ultracapacitor at three different ambient temperatures of 10, 20, and 30 °C during the 10 and 100 test cycles of Fig. 4, respectively. The solid curves are the temperatures at a point in the central core region, whose coordinates are $x = 3$ cm, $y = 2.6$ cm, and $z = 4.5$ cm. The curves with open circles are the temperatures of the terminal on the top cover. As shown in Fig. 5(a), the temperature of the core region responds sensitively to the heat generation during charge and discharge, because the heat generation occurs throughout the core region during the charge and discharge processes [10]. By contrast, the temperature of the terminal responds

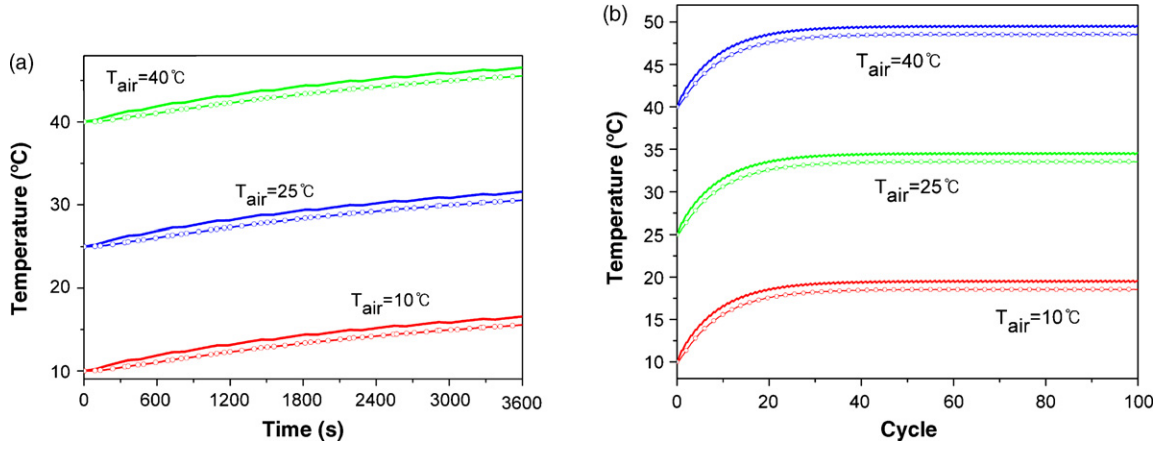

Fig. 5. Temperature transition of cell during (a) 10 cycles and (b) 100 cycles. Solid curves are temperatures of core region and curves with open circles are temperatures of terminal.

Table 3
Maximum and minimum temperatures for different ambient temperatures and numbers of cycles

Ambient temperature (°C)	Number of cycles	Maximum temperature (°C)	Minimum temperature (°C)
	10	16.64	14.10
10	30	19.28	17.84
	50	19.56	18.16
	10	31.64	29.09
25	30	34.28	32.84
	50	34.56	33.16
	10	46.64	44.09
40	30	49.27	47.84
	50	49.56	48.16

less sensitively to the charge and discharge processes due to the time lag required for heat conduction between the core region, where the heat is generated, and the terminal on the top cover, where the heat is dissipated to the atmosphere by convection. During cycling, the temperature of the ultracapacitor increases during the first 50 test cycles, after which it reaches a periodic steady-state in which the heat generation due to charge and discharge balances the heat dissipation through the surface of the cell, as can be observed in Fig. 5(b).

The temperature distribution on the surface of the ultracapacitor and the isothermal surface distribution in the interior of the ultracapacitor at the end of the 50th test cycle are shown in Figs. 6(a and b), respectively. The temperature around the core region is higher than that near the top cover. Since the temperature gradient is perpendicular to the isothermal surface, we can estimate the direction of the heat flux, which is the same as that of the temperature gradient shown in Fig. 6. The maximum and minimum temperatures for the different ambient temperatures and numbers of cycles are listed in Table 3. Both of these temperatures are observed to increase with increasing ambient temperature (as would be expected). Although the temperature increases with increasing number of cycles up to 50 cycles, as shown in Fig. 5(b), the increase is not significant after the initial 30 cycles, as shown in Table 3.

5. Conclusions

A three-dimensional modelling approach has been used to study the effects of the operating and ambient conditions on the thermal behaviour of a NESSCAP 2.7 V/3500 F ultracapacitor cell for a 42-V automotive electrical system. The heat generation rates of the ultracapacitor during charge and discharge are measured with a calorimeter. For the modelling, test cycles consisting of idle-stop, acceleration, driving, and regenerative-braking are applied. The transient temperature distribution of the ultracapacitor during 100 test cycles is obtained using the finite element method with an implicit predictor-multicorrector algorithm. The results show that the temperature of the ultracapacitor increases during the first 50 test cycles, after which it reaches a periodic steady-state, and that it also increases with increasing ambient temperature. The modelling presented in this study may be useful for the development of a thermal-management strategy for 42-V automotive electrical systems, in order to maintain the operating temperature and the temperature uniformity of the ultracapacitor module within a suitable range.

Acknowledgements

This work was supported by the Ministry of Commerce, Industry, and Energy of the Republic of Korea under the Technology Development Program of the 42-V automotive electrical system. One of the authors (C.B. Shin) acknowledges partial financial support provided by the Korea Science and Engineering Foundation (KOSEF R01-2006-000-10239-0) and the FOI Corporation.

References

[1] C. Ashtiani, R. Wright, G. Hunt, J. Power Sources 154 (2006) 561–566.
[2] A. Burke, J. Power Sources 91 (2000) 37–50.
[3] A. Burke, Proceedings of the Second International Advanced Automotive Battery Conference, Las Vegas, NV, February, 2002.
[4] J.N. Marie-Francoise, H. Gualous, R. Outbib, A. Berthon, J. Power Sources 143 (2005) 275–283.
[5] P. Bentley, D.A. Stone, N. Schofield, J. Power Sources 149 (2005) 288–294.
[6] A.W. Stienecker, T. Stuart, C. Ashtiani, J. Power Sources 156 (2006) 755–762.
[7] M. Anderman, J. Power Sources 127 (2004) 2–7.
[8] P.T. Moseley, D.A.J. Rand, J. Power Sources 133 (2004) 104–109.
[9] S.C. Chen, C.C. Wan, Y.Y. Wang, J. Power Sources 140 (2005) 111–124.
[10] Y. Chen, J.W. Evans, J. Electrochem. Soc. 141 (1994) 2947–2955.
[11] Y. Chen, J.W. Evans, Electrochim. Acta 39 (1994) 517–526.
[12] D.R. Lide, CRC Handbook of Chemistry and Physics, CRC Press, Boca Raton, FL, 1988.
[13] R.H. Perry, D.W. Green, Chemical Engineers' Handbook, McGraw-Hill, New York, NY, 1999.
[14] J. Brandrup, E.H. Immergut, Polymer Handbook, second ed., Wiley, New York, NY, 1975.
[15] T.J.R. Hughes, K.S. Pister, R.L. Taylor, Comput. Mech. Appl. Mech. Eng. 17/18 (1982) 159.